SPECIAL ISSUE
Dedicated to
ECOS 2006

19th International Conference on Efficiency, Cost, Optimization, Simulation and Environmental Impact of Energy Systems

AGHIA PELAGIA, CRETE, GREECE
JULY 12–14, 2006

Guest Editors
C. A. Frangopoulos, C.D. Rakopoulos, and G. Tsatsaronis

Coordinating Editor
Noam Lior

Available online at
ScienceDirect
www.sciencedirect.com

Available online at www.sciencedirect.com
ScienceDirect
ELSEVIER
Energy 33 (2008) 300–310
ENERGY
www.elsevier.com/locate/energy

Modeling and dynamics of an autothermal JP5 fuel reformer for marine fuel cell applications ☆

Vasilis Tsourapas[a,*], Jing Sun[a], Anthony Nickens[b]

[a] University of Michigan, NAME Department, 2600 Draper Rd, Ann Arbor, MI, 48109, USA
[b] Ceramatec Inc., 2425 South 900 West, Salt Lake City, UT 84119, USA

Received 30 December 2006

Abstract

In this work, a dynamic model of an integrated autothermal reformer (ATR) and proton exchange membrane fuel cell (PEM FC) system and model-based evaluation of its dynamic characteristics are presented. The ATR reforms JP5 fuel into a hydrogen rich flow. The hydrogen is extracted from the reformate flow by a separator membrane (SEP), then supplied to the PEM FC for power generation. A catalytic burner (CB) and a turbine are also incorporated to recuperate energy from the remaining SEP flow that would otherwise be wasted. A dynamic model of this system, based on the ideal gas law and energy balance principles, is developed and used to explore the effects of the operating setpoint selection of the SEP on the overall system efficiency. The analysis reveals that a trade-off exists between the SEP efficiency and the overall system efficiency. Finally the open loop system simulation results are presented and conclusions are drawn on the SEP operation.

Keywords: Autothermal reforming; JP5; Fuel cell; Marine; Dynamics

1. Introduction

Given the existing fueling infrastructure and the relatively lenient space restrictions in marine applications, combined fuel reforming (FR) and fuel cell (FC) technologies are an attractive option for shipboard power systems. They not only capitalize on the high FC efficiency, but also allow tight integration of multiple thermal sources and heat loads, making them an ideal candidate for combined heat and power marine applications. For all-electric ships, the FR–FC systems have the additional benefits of reduced thermal and acoustic signature and improved reconfigurability. These expected advantages have motivated intensive research activities around the world to develop feasible FR–FC shipboard systems.

As an emerging technology, FR–FC systems are still at the early stage of development and many technical issues are yet to be addressed before this technology becomes mature and ready for shipboard applications. The main challenges fall into two distinct categories: materials and operational issues. The issues associated with the materials are mainly concerned with the cost and durability, while operational issues involve the transient requirements and load following capabilities. In this work we use analytical and numerical tools to analyze primarily the performance and limitations of an integrated FR–FC system in order to address its operational issues.

The system investigated is an FR–FC combination based on autothermal reforming (ATR) technology and a proton exchange membrane fuel cell (PEM FC). A schematic of the system is shown in Fig. 1. The reformer utilizes JP5 jet fuel and converts it into a pure hydrogen stream via autothermal reforming, before it is used in the fuel cell. A desulphurizer (DS), a water gas shift (WGS) reactor and a separator (SEP) ensure that when the stream reaches the fuel cell, it will be almost 100% hydrogen. The separator (SEP) plays a critical role in purifying the reformate. It incorporates a palladium-coated membrane to extract hydrogen present in the reformate flow via diffusion before feeding it to the FC, while the remaining flow is sent

☆ This work is funded the US Navy under contract N00014-06-1-0209.
*Corresponding author. Tel.: +1 734 277 5258.
E-mail address: djvas@umich.edu (V. Tsourapas).

0360-5442/$ - see front matter © 2007 Elsevier Ltd. All rights reserved.
doi:10.1016/j.energy.2007.08.006

Nomenclature

A	separator membrane area
A_p	heat exchanger plate active area
d_o	orifice coefficient (kg/s$\sqrt{Pa}$)
F	Faraday's constant (Cb/mole)
H	enthalpy (J/kg)
H_f	enthalpy of formation (J/kg)
HU	fuel cell hydrogen utilization
in	property of incoming flow (subscript)
I_{st}	fuel cell stack current (A)
J_s	shaft rotational inertia (kg m^2)
K	membrane permeability coefficient
k	number of cells in FC
$LMTD$	log mean temperature difference
m	mass (kg)
M	molar weight (kg/mole)
N	rotational speed (rpm)
$n_{(\cdot)}$	molar rate of species $(\cdot)$
out	property of outgoing flow (subscript)
p	power (W)
P	pressure (Pa)
Q	heat released (J/kg)
q_{LHV}	lower heating value (J/mole)
R	universal gas constant (J/kg K)
T	temperature (K)
U	heat transfer coefficient (W/m^2 K)
V	volume (m^3)
W	flow rate (kg/s)
x	molar fraction
y	mass fraction

Greek letters

η	efficiency (%)
λ_{i2j}	molar ratio of two species

Abbreviations for system components

ATR	autothermal reformer
CB	catalytic Burner
CMP	compressor
DS	desulphurizer
FC	fuel cell
FR	fuel reformer
GEN	generator
HEX	heat exchanger
M	motor
MIX	mixer
SEP	separator
sepHP	separator high pressure side
sepLP	separator low pressure side
TRB	turbine
WGS	water gas shift

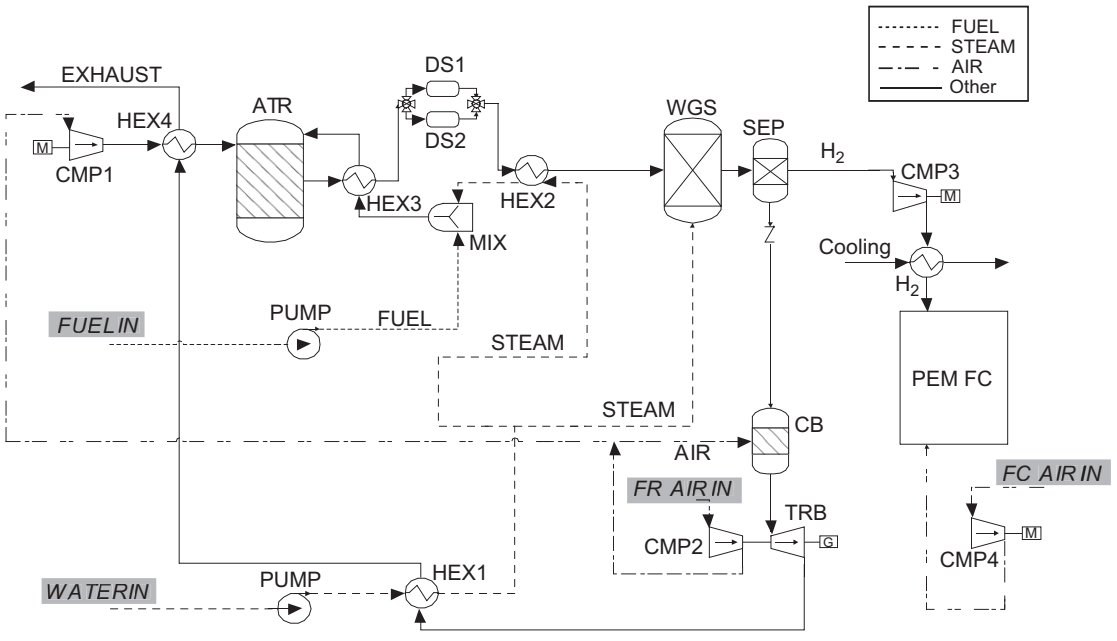

Fig. 1. ATR JP5 reformer schematic.

to a catalytic burner and gas turbine in order to recuperate energy.

Most of the work on autothermal reformer systems published in the literature is focused on hydrogen production and the associated optimization problems. Modeling activities and experimental efforts are mainly aimed towards determining the reactant flows and inlet gas composition at steady state operation that achieve maximum

hydrogen production and maintain safe operating conditions for the reformer [1–3]. The effects of operating parameters such as the steam-to-fuel and air-to-fuel ratios, flow rates and temperature on the ATR products and efficiency are considered in [4–6] and optimal values are determined. To maintain the desired steady state operating conditions and assure safe system operation, especially when the load is changed, precise control of hydrogen production and reactor temperature is required. Analysis of the transient behavior of autothermal reformers also indicates, implicitly or explicitly, the need for accurate control of reactant flows in order to maintain system operational integrity and avoid overheating or fuel starvation [7,8].

Following these works, the goals of our research are twofold: namely (a) to develop a dynamic model of the system that is amendable to existing control system design tools and methodologies and (b) to perform model-based analysis to gain insights on the system dynamic operation. A thermodynamic, low order and control oriented model of the system is developed. Critical parameters that affect its load following capabilities and optimal operating setpoints corresponding to the maximum system efficiency are determined via open loop analysis. The lessons learned and the tools developed from the open loop analysis will facilitate feedback control design in future work, therefore contributing towards the realization of a highly efficient and robust fuel cell based shipboard power plant.

2. System overview and operation

For the system investigated in this paper, the inputs are JP5 fuel and air to the fuel reformer (*FUELIN*, *FR AIRIN*, respectively), air to the fuel cell (*FC AIRIN*) and water into the reformer (*WATERIN*) as highlighted on Fig. 1. The actuators delivering the fuel and water flows are two separate liquid phase pumps while compressors are used for providing the air to the system. Steam is created by utilizing the system exhaust and the ATR outlet heat via two heat exchangers (*HEX*1, *HEX*2). The steam is mixed with the incoming fuel in the mixer (*MIX*) and the mixed fuel and steam flow is further heated in *HEX*3 and fed into the ATR. The air flow required for the ATR operation is supplied by two compressors (CMP1 and CMP2, driven by a motor and by the turbine shaft, respectively) and heated by HEX4 before entering the reactor.

Given a generic hydrocarbon fuel denoted as C_nH_m, the main reactions that can take place in the ATR reformer are partial and total oxidation (POX, TOX), partial and total steam reforming (PSR, TSR), WGS and methane formation (MF) [2]:

$$C_nH_m + \frac{n}{2}O_2 \rightleftharpoons nCO + \frac{m}{2}H_2 \quad (POX), \tag{1}$$

$$C_nH_m + \left(n + \frac{m}{4}\right)O_2 \rightleftharpoons nCO_2 + \frac{m}{2}H_2O \quad (TOX), \tag{2}$$

$$C_nH_m + nH_2O \rightleftharpoons nCO + \left(n + \frac{m}{2}\right)H_2 \quad (PSR), \tag{3}$$

$$C_nH_m + 2nH_2O \rightleftharpoons nCO_2 + \left(2n + \frac{m}{2}\right)H_2 \quad (TSR), \tag{4}$$

$$CO + H_2O \rightleftharpoons CO_2 + H_2 \quad (WGS), \tag{5}$$

$$CO + 3H_2 \rightleftharpoons CH_4 + H_2O \quad (MF). \tag{6}$$

For the case we are interested in, the average formula for JP5 is $C_{12}H_{23}$. The rate of each reaction and thus the hydrogen production is dictated by the reactor temperature (T^{atr}), the oxygen-to-fuel molar ratio (λ_{O_2F}) and the steam-to-fuel molar ratio (λ_{S_2F}). These ratios are defined as

$$\lambda_{O_2F} = n_{O_2}/n_{C_nH_m}, \quad \lambda_{S_2F} = n_{H_2O}/n_{C_nH_m} \tag{7}$$

where $n_{(\cdot)}$ is the molar flow of species $(\cdot)$.

The ATR outlet flow, after passing through *HEX*3, is desulphurized in *DS*1 or *DS*2 and reaches the WGS reactor where only reactions (5) and (6) take place. A portion of the steam produced by HEX1 is utilized in the WGS to further promote the H_2 production (5) while a portion of the hydrogen will react with CO in the methane formation reaction (6). By controlling the WGS temperature through the carbon-to-steam inlet ratio, one can minimize the methane formation and maximize H_2 yield in the WGS reactor.

The reformate exiting the WGS will then reach the separator (*SEP*), a hydrogen extraction device made of a palladium based diffusion membrane. Its primary function is to extract the hydrogen from the incoming flow and produce an ultra-pure hydrogen flow that can be utilized by a low temperature PEM FC. The remaining reformate, after the hydrogen has been extracted, is burned in the CB with air, converting the remaining chemical energy to heat. Then, the CB outlet flow passes through a turbine where the remaining energy in the exhaust is recuperated for air compression and power generation via the attached generator set.

A model of the system described here is developed, with its main component sub-models presented in the next section. The models for the FC and DS components, which were developed [9] and used in our previous work [10], are included here for completeness.

3. System modeling

The model is developed with a focus on capturing the dynamic behavior associated with the flow, pressure and temperature of the integrated system. The main assumptions are that all gases obey the ideal gas law and all gas mixtures are perfect mixtures with homogenous composition. These assumptions allow the application and development of a lumped parameter model suitable for open and closed loop control oriented analysis. It is also assumed that there are no heat losses to the environment.

The model developed in this paper is largely based on first principles. Since the technology is fast evolving,

material development has not been stabilized yet and data for relevant hardware are very limited and not representative. At this stage any model-based analysis using a specific hardware configuration may not be generalizable once the hardware, including materials and manufacturing process, changes. Therefore, we choose to focus on a generic model whose parameters can be calibrated to reflect a specific system, once the data becomes available.

It should be pointed out that the system model presented in this paper has not been validated yet with experimental data, mainly because the system level hardware does not exist according to the best knowledge of the authors. For those components that are readily available, such as the heat exchanger and mixer, models that have been well developed and widely accepted [11] are adopted here. The system model, even without full experimental validation, can provide a useful analysis tool to guide system integration and control design. Two particularly useful applications include system sensitivity analysis with respect to the parameters and the evaluation of trade-offs of component level versus system level optimization.

In the remainder of the paper, it is assumed that the flow rate exiting one volume can be calculated based on the orifice flow equation

$$W^{vol} = d_o\sqrt{P^{vol} - P^{next\ vol}}, \tag{8}$$

where $d_o = W_{nom}/\sqrt{\Delta P_{nom}}$. The flow rate exiting a volume, W^{vol}, is given as a function of the pressure of that volume, P^{vol}, and the pressure of the downstream (next) volume, $P^{next\ vol}$. The flow is assumed turbulent and the rate is governed by W_{nom} and ΔP_{nom}, which are the nominal air flow rate and the nominal pressure drop of the orifice, respectively. These nominal values (i.e., d_o) depend on the orifice size, geometry, shape, etc., and can be calibrated if flow and pressure data are available.

3.1. Autothermal reformer model

For the ATR model, we consider both temperature and pressure dynamics which can be captured by balancing the energy flow as follows:

$$\frac{\mathrm{d}P^{atr}}{\mathrm{d}t} = \frac{RT_{atr}}{M^{atr}V^{atr}}\left(\sum W_{in}^{atr} - W_{out}^{atr}\right) + \frac{Rm^{atr}}{M^{atr}V^{atr}}\left(\frac{\mathrm{d}T^{atr}}{\mathrm{d}t}\right), \tag{9}$$

$$m_{bed}^{atr}c_{p_{bed}}^{atr}\frac{\mathrm{d}T^{atr}}{\mathrm{d}t} = \Delta H_{atr}, \tag{10}$$

where $(\cdot)_{bed}^{atr}$ are properties of the ATR catalyst bed, the mass in the ATR, m^{atr}, can be determined using the states P^{atr} and T^{atr} as

$$m^{atr} = \frac{P^{atr}V^{atr}M^{atr}}{RT^{atr}}, \tag{11}$$

and ΔH_{atr} is the difference in absolute enthalpy between the ATR inlet and outlet composition, expressed as

$$\begin{aligned}\Delta H_{atr} &= H_{in}^{atr} - H_{out}^{atr}\\ &= (H_{T_{in}^{atr}} - H_{T_{ref}} + H_f)_{in}\\ &\quad - (H_{T_{out}^{atr}} - H_{T_{ref}} + H_f)_{out},\end{aligned} \tag{12}$$

where $H_{T_{in}^{atr}}$, $H_{T_{out}^{atr}}$, $H_{T_{ref}}$ and H_f are the enthalpy of the inlet flow at the inlet temperature, the enthalpy of the outlet flow at the ATR temperature, the enthalpy at the reference temperature and the enthalpy of formation, respectively. The enthalpy calculation for the inlet, H_{in}^{atr}, and outlet, H_{out}^{atr}, requires the knowledge of the corresponding flow composition. While the composition for the inlet flow is known, the composition for the outlet depends on the reactions taking place inside the reactor and therefore the temperature and inlet conditions. In this work, the outlet composition is determined by pre-calculated lookup tables which map the ATR products to the ATR inlet conditions, namely T^{atr}, λ_{O_2F} and λ_{S_2F}. These maps are created using the GasEq© software [12] that utilizes the Gibbs minimization algorithm to calculate the outlet composition. The inputs to the maps have the range of $\lambda_{O_2F} = [2, 18]$ with an incremental step of 0.2, $\lambda_{S_2F} = [2, 18]$ with an incremental step of 0.2 and $T^{atr} = [600, 1400]$ with an incremental step of 50 K. The products predicted by the maps include H_2, CO, CO_2, CH_4, O_2, H_2O, SO_2, H_2S, and N_2. For illustration purpose, two examples of those pre-calculated maps are shown for selected operating conditions in Fig. 2 for H_2 and CO. It should be noted that the dependence of the reaction products to the reactor pressure (P^{atr}) is ignored, since its effects are not significant compared to T^{atr}, λ_{O_2F} and λ_{S_2F}.

Given the molar flow rates determined according to the maps, the molar fraction of the ATR products is calculated as:

$$x_i = \frac{n_i}{\sum_{j=1}^{9} n_j}. \tag{13}$$

A schematic of the ATR model, depicting the signal flows and involved inputs, outputs and states, is shown in Fig. 3.

3.2. Water gas shift reactor model

Given that the molar and mass fractions of the flow entering the WGS reactor are the same as the ones exiting the ATR, we can express the mass balance dynamics by applying the mass conservation as

$$\frac{\mathrm{d}m^{wgs}}{\mathrm{d}t} = \sum W_{in}^{wgs} - W_{out}^{wgs} \tag{14}$$

and the temperature dynamics

$$\begin{aligned}m_{bed}^{wgs}c_{p_{bed}}^{wgs}\frac{\mathrm{d}T^{wgs}}{\mathrm{d}t} &= (W_{in}^{wgs}c_{p_{in}}^{wgs}(T_{in}^{wgs} - T_{ref}))\\ &\quad - W_{out}^{wgs}c_{p_{out}}^{wgs}(T^{wgs} - T_{ref})\\ &\quad + Q_{wgs} + Q_{mf}.\end{aligned} \tag{15}$$

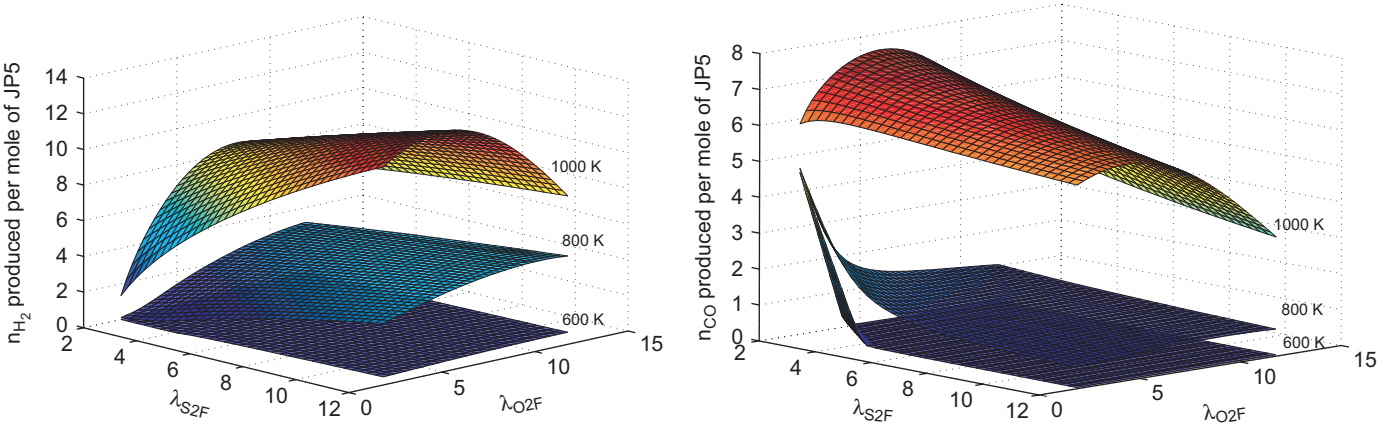

Fig. 2. ATR H_2 and CO production per mole of JP5 fuel at 600, 800 and 1000 K.

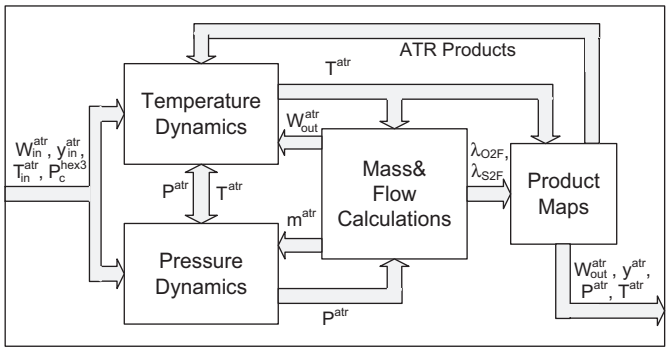

Fig. 3. ATR reactor model.

The heat released by the WGS and the MF reactions (Q_{wgs}, Q_{mf}, respectively) are obtained using the enthalpy of formation per mole of CO reacting in the corresponding reactions. In this work, the amount of CO reacting is assumed to be a constant percentage of the total amount of CO entering the WGS reactor.

3.3. Catalytic burner model

The catalytic burner (CB) is the device where the reformate flow, after a significant amount of H_2 has been extracted by the SEP, is burned with the addition of air to increase the flow temperature before it enters the turbine (TRB). In modeling the CB, the dynamics taken into account are the mass dynamics via the mass balance

$$\frac{\mathrm{d}m^{cb}}{\mathrm{d}t} = \sum W_{in}^{cb} - W_{out}^{cb}, \tag{16}$$

and the temperature dynamics via the energy balance

$$m_{bed}^{cb} c_{p,bed}^{cb} \frac{\mathrm{d}T^{cb}}{\mathrm{d}t} = (W_{in}^{cb} c_{P,in}^{cb} (T^{in} - T_{ref})) - W_{out}^{cb} c_{P,out}^{cb} (T^{out} - T_{ref}) + Q^{cb}, \tag{17}$$

where $c_{p,bed}^{cb}$, $c_{P,in}^{cb}$ and $c_{P,out}^{cb}$ are the constant-pressure specific heats of the CB catalyst, the CB inlet flow and the CB outlet flow and are calculated using the NASA polynomials[1] [13]. Q^{cb} is the heat released by burning the hydrogen and the methane present in the flow and is expressed as

$$Q_r^{cb} = q_{LHV_{\mathrm{H_2}}} W_{\mathrm{H_2}}^{cb} + q_{LHV_{\mathrm{CH_4}}} W_{\mathrm{CH_4}}^{cb} \tag{18}$$

assuming there is enough air in the CB to burn all the H_2 and CH_4 entering the CB. Note, that due to the small concentration of CO (less than 1%) and its low heating value compared to H_2 and CH_4, the contribution of CO oxidation to the CB temperature is not considered. The ideal gas law is then used to calculate the pressure in the CB as

$$P^{cb} = \frac{1}{V^{cb}} \frac{m^{cb}}{M^{cb}} R T^{cb}. \tag{19}$$

3.4. Compressor and turbine model

The shaft dynamics are the only dynamics considered in the CMP/TRB set and are determined by the power generated by the turbine p^{trb}, the power consumed by the compressor p^{cmp} and the power used for the generator p^{gen} as

$$\frac{\mathrm{d}N}{\mathrm{d}t} = \frac{p^{trb}\eta_m - p^{cmp} - p^{gen}}{J_s N (2\pi/60)^2}, \tag{20}$$

where N is the shaft rotational speed, J_s is the shaft rotational inertia and η_m is the mechanical efficiency of the turbine that accounts for energy losses due to friction. A typical value for η_m is 0.95. The factor $(2\pi/60)^2$ is a result of unit conversion to *rpm*.

The compressor outlet temperature and required power can be expressed as

$$T_{out}^{cmp} = T_{in}^{cmp} \left(1 + \frac{1}{\eta_{c,is}} \left(\left(\frac{P_{out}^{cmp}}{P_{in}^{cmp}} \right)^{(\gamma-1)/\gamma} - 1 \right) \right), \tag{21}$$

[1] All the specific heats noted in this paper are calculated as a function of temperature using the NASA polynomials.

$$p^{cmp} = W^{cmp} c_p^{cmp} T_{in}^{cmp} \frac{1}{\eta_{c,is}} \left(\left(\frac{P_{out}^{cmp}}{P_{in}^{cmp}} \right)^{(\gamma-1)/\gamma} - 1 \right), \tag{22}$$

where $\eta_{c,is}$ is the isentropic efficiency of the compressor and W^{cmp} the flow through the compressor; both are determined through the compressor maps given the operating pressure ratio.

Similarly, the turbine outlet temperature and produced power are expressed as

$$T_{out}^{trb} = T_{in}^{trb} \left(1 - \eta_{t,is} \left(1 - \left(\frac{P_{out}^{trb}}{P_{in}^{trb}} \right)^{(\gamma-1)/\gamma} \right) \right), \tag{23}$$

$$p^{trb} = W^{trb} c_p^{trb} T_{in}^{trb} \eta_{t,is} \left(1 - \left(\frac{P_{out}^{trb}}{P_{in}^{trb}} \right)^{(\gamma-1)/\gamma} \right), \tag{24}$$

where $\eta_{t,is}$ is the isentropic efficiency of the turbine and W^{trb} the flow through the turbine, which can be determined given the turbine maps and the operating pressure ratio.

3.5. Desulphurizer model

The pressure of the gas in the DS is governed by the ideal gas law. The DS is considered just as a volume since the sulphur removed from the flow is only a very small faction (1000 ppm), which does not affect the mass balance significantly. The pressure dynamics are derived using the ideal gas law:

$$\frac{dP^{ds}}{dt} = \frac{RT^{ds}}{M^{ds} V^{ds}} (W_{in}^{ds} - W_{out}^{ds}), \tag{25}$$

where W_{out}^{ds} is the rate of mass flow exiting the DS, and is calculated as a function of P^{ds} and P^{next} using the orifice Eq. (8). The temperature of the gas, T^{ds}, is assumed constant and equal to the incoming flow temperature. The efficiency and effects of sulphur removal are not considered in detail in this work.

3.6. Fuel cell anode model

Mass conservation is used to derive the pressure dynamics in the anode volume. Since pure hydrogen flow is fed into the anode, the only pressure dynamics considered are the total pressure dynamics expressed as

$$\frac{dP^{an}}{dt} = \frac{RT^{an}}{M^{an} V^{an}} (W_{in}^{an} - W_{out}^{an} - W_{H_2}^{react}). \tag{26}$$

The rate of hydrogen reacted is a function of stack current, I_{st}, through the electrochemistry principle [14]:

$$W_{H_2}^{react} = M_{H_2} \frac{k I_{st}}{2F}. \tag{27}$$

An important variable used to monitor the performance of the system is the hydrogen utilization, HU, that can be calculated by

$$HU = \frac{H_2 \text{ reacted}}{H_2 \text{ supplied}} = \frac{W_{H_2}^{react}}{W_{H_2}^{supplied}}. \tag{28}$$

3.7. Heat exchanger model

The dynamics considered in the heat exchangers include both pressure and temperature dynamics on the hot and the cold side. The mass balance principle and the ideal gas law are used to model the pressure and temperature dynamics in each side of the heat exchanger. Note that these equations apply both to the cold (c) and the hot (h) side of the HEX and that the HEX used has a co-flow stream configuration.

The states in the HEX include the mass and temperature in each of the cold and hot sides. The mass balance in the HEX is expressed as

$$\frac{dm_{c/h}^{hex}}{dt} = (W_{in}^{hex} - W_{out}^{hex}). \tag{29}$$

The energy balance, using temperature as the state, yields

$$\begin{aligned} m_{bed}^{hex} c_{p_{bed}}^{hex} \frac{dT_{c/h}^{hex}}{dt} = {} & W_{in}^{hex} c_{p_{in}}^{hex} (T_{c/h}^{in} - T_{ref}) \\ & - W_{out}^{hex} c_{p_{out}}^{hex} (T_{c/h}^{hex} - T_{ref}) \\ & \pm UA_p (LMTD), \end{aligned} \tag{30}$$

where the (+) or (−) sign in front of the $LMDT$ is used to denote the heat increase (+) or decrease (−) due to the heat transfer, for the cold and hot sides, respectively. The term $LMTD$ represents the heat transfer rate between the hot side and cold side of a heat exchanger. For a co-flow HEX, it is given by [15]

$$LMTD = \frac{(T_h^{in} - T_c^{in}) - (T_h^{out} - T_c^{out})}{\ln[(T_h^{in} - T_c^{in})/(T_h^{out} - T_c^{out})]}. \tag{31}$$

The ideal gas law is used to calculate the pressure as

$$P_{c/h}^{hex} = \frac{m_{c/h}^{hex} R T_{c/h}^{hex}}{M_{c/h}^{hex}}. \tag{32}$$

3.8. Mixer model

The mixer is modeled as a volume where no reactions occur but its overall temperature and pressure are a function of the partial pressures of the steam and fuel and their corresponding temperatures. Thus, in the MIX the partial pressures of fuel and steam can be expressed as

$$\frac{dP_{fuel}^{mix}}{dt} = \frac{RT^{mix}}{M_{fuel} V^{mix}} (W_{fuel,in}^{mix} - y_{fuel}^{mix} W_{out}^{mix}), \tag{33}$$

$$\frac{dP_{H_2O}^{mix}}{dt} = \frac{RT^{mix}}{M_{H_2O} V^{mix}} (W_{H_2O,in}^{mix} - y_{H_2O}^{mix} W_{out}^{mix}), \tag{34}$$

where y_f^{mix} and $y_{H_2O}^{mix}$ are the mass fractions of fuel and steam in the MIX, respectively, and are defined as

$$y_{fuel}^{mix} = \frac{1}{1 + (M_{H_2O} P_{H_2O}^{mix} / M_{fuel} P_{fuel}^{mix})}, \tag{35}$$

$$y_{H_2O}^{mix} = \frac{1}{1 + (M_{fuel} P_{fuel}^{mix} / M_{H_2O} P_{H_2O}^{mix})}. \tag{36}$$

Furthermore, using the energy balance principle we can express the temperature dynamics as

$$m_{bed}^{mix} c_{p,bed}^{mix} \frac{dT_{out}^{mix}}{dt} = W_{in}^{mix} c_{P,in}^{mix} (T_{in}^{mix} - T_{ref}) - W_{out}^{mix} c_{P,out}^{mix} (T_{out}^{mix} - T_{ref}). \tag{37}$$

Using the orifice equation, the flow out of the MIX can be calculated as

$$W_{out}^{mix} = d_o^{mix} \sqrt{(P_{fuel}^{mix} + P_{H_2O}^{mix}) - P_c^{hex3}}. \tag{38}$$

3.9. Separator model

A key component in this FR–FC system is the SEP membrane. The palladium based membrane is used to separate hydrogen from the incoming flow, therefore safeguarding the FC from being poisoned by CO or impurities in the inlet flows. One challenge of integrating a SEP membrane into a FR system is the high operating pressure requirement. Since the pressure differential across the membrane is the driving force that makes the SEP operate efficiently, an average system operating pressure of 7 atm is required.

A simplified schematic of the SEP with a planar membrane is shown in Fig. 4. For increased membrane area and separation efficiency, a tubular membrane is commonly utilized [16]. The separation efficiency can be defined as

$$\eta_{sep} = \frac{H_2 \text{ exiting LP side}}{H_2 \text{ entering HP side}} = \frac{W_{H_2\ out}^{sepLP}}{W_{H_2\ in}^{sepHP}}. \tag{39}$$

The empirical law that allows the calculation of the hydrogen going through the membrane (W_{th}) can be expressed as [16,17]

$$W_{th} = KA((P_{H_2}^{sepHP})^{0.6} - (P_{H_2}^{sepLP})^{0.6}), \tag{40}$$

where K is the membrane permeability coefficient, A is the membrane area and $P_{H_2}^{sepHP}$, $P_{H_2}^{sepLP}$ are the partial pressures of H_2 in the HP and LP sides of the separator, respectively. Note that since the LP side is pure hydrogen, the partial pressure of H_2 in the LP side is equal to the total pressure on that side. Also, the exponent 0.6 in (34) was found to best match the experimental data from the hardware manufacturer.

Furthermore, it is assumed that the flow entering the SEP (i.e., the flow exiting the WGS reactor) is at chemical equilibrium, hence no reactions take place in the SEP. Consequently, the temperature is maintained constant and no temperature dynamics are considered, i.e., the temperatures in the LP and HP side are considered equal ($T^{sepHP} = T^{sepLP} = T^{sep}$). Since a separate volume was considered for the WGS reaction, the use of this assumption is justified.

Now, referring to Fig. 4 and using the ideal gas law, the pressure dynamics in the HP and LP volumes can be expressed as

$$\dot{P}^{sepHP} = \frac{RT^{sep}}{M_{HP}^{sep} V_{HP}^{sep}} (W_{in}^{sepHP} - W_{out}^{sepHP} - W_{th}), \tag{41}$$

$$\dot{P}_{H_2}^{sepHP} = \frac{RT^{sep}}{M_{H_2} V_{HP}^{sep}} (W_{H_2\ in}^{sepHP} - W_{H_2\ out}^{sepHP}), \tag{42}$$

$$\dot{P}^{sepLP} = \frac{RT^{sep}}{M_{H_2} V_{LP}^{sep}} (W_{th} - W_{out}^{sepLP}) \tag{43}$$

where $W_{H_2\ out}^{sepHP}$ is the flow rate of hydrogen exiting the HP side of the SEP given by

$$W_{H_2\ out}^{sepHP} = W_{out}^{sepHP} \frac{P_{H_2}^{sepHP} M_{H_2}}{P^{sepHP} M^{sepHP}} + W_{th}. \tag{44}$$

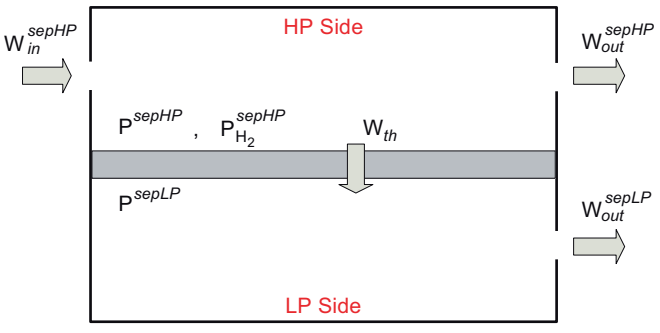

Fig. 4. Separator membrane schematic.

4. SEP setpoint selection and efficiency trade-off analysis

Given that the FC is more efficient than the turbine/generator set, one would think that, as far as power generation is concerned, it is advantageous to extract as much hydrogen as possible to feed the FC and capitalize its high efficiency. However, the system is designed to be autonomous, thus all compressors present in the system are powered by the FC power output or the turbine. Maximizing the SEP hydrogen extraction by increasing the HP side pressure will lead to increased parasitic losses due to the increased system average operating pressure.

The goal in this section is to define the SEP pressure that yields high hydrogen separation without causing the overall system efficiency deteriorating. Note that the SEP HP pressure dictates the overall system pressure, since it is downstream of all the reactors. The SEP operating pressure also dictates the amount of hydrogen extracted and thus it

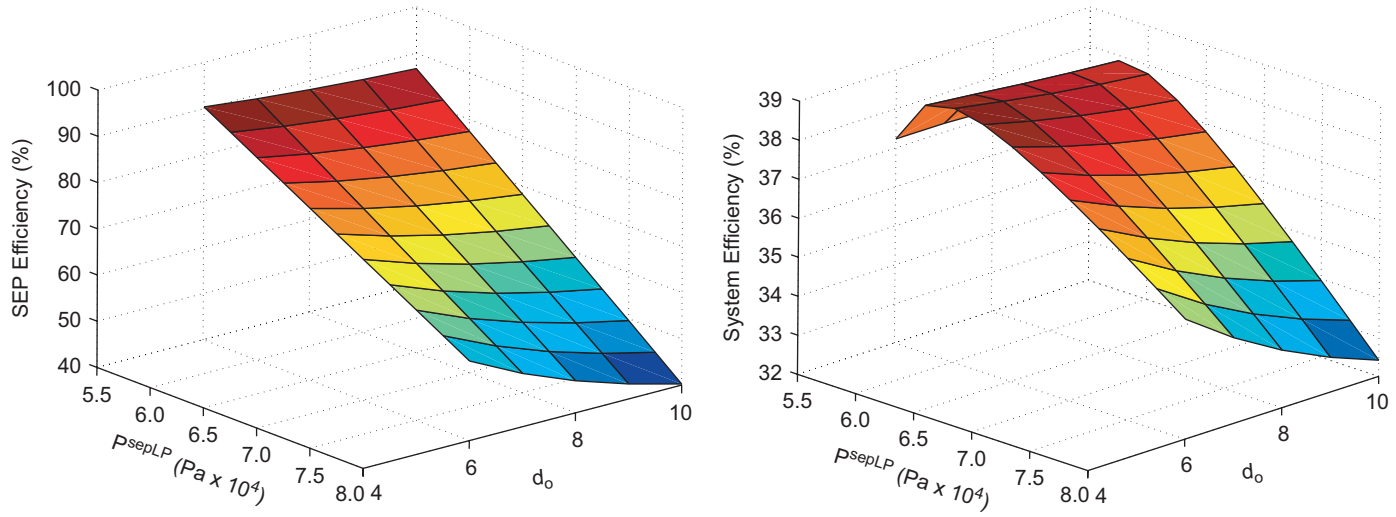

Fig. 5. Separator and system efficiencies for variable pressures and orifice coefficients.

is a crucial parameter in defining the overall system efficiency expressed as

$$\eta_s = \frac{Net\ power}{Fuel\ energy} = \frac{p^{fc} + p^{gen} - p^{cmp}}{W_f^{used} LHV_f}. \quad (45)$$

In order to control the hydrogen extraction and optimize the system efficiency, two individual actuators are available. One is the compressor on the LP side of the SEP which controls the pressure on that side (P^{sepLP}) and the other is the valve present on the outlet of the HP side (d_o). Decreasing the operating setpoint for both P^{sepLP} and d_o will result in increased hydrogen extraction given the increase in pressure difference between LP and HP, but the challenge is to define up to what point increasing hydrogen extraction is useful to the system's efficiency.

In order to define the setpoints for the SEP for a given combination of fuel, air and steam inputs, the maps shown in Fig. 5 are constructed. The efficiencies for the SEP and the overall system are plotted with respect to the LP side pressure and the HP outlet orifice coefficient d_o. Note that the orifice coefficient is analogous to the opening of the valve.

For the case shown in Fig. 5, the fuel, air and steam flows are 0.03, 0.30 and 0.04 kg/s, respectively. The optimum overall efficiency is 38.6%, achieved at LP pressure of 68 kPa and d_o equal to 4 (Fig. 5). The corresponding SEP efficiency, at the same LP pressure and d_o is at 87% (Fig. 5). Attempt to further increase the SEP efficiency by decreasing either the LP pressure or the orifice area results in increased compressor power consumption, which eventually results in system efficiency reduction.

Furthermore it can be seen from Fig. 5 that decreasing the LP pressure is a more effective way of boosting the overall efficiency compared to decreasing the HP orifice valve area. In building the reformer system though, the actual operating pressures will be dictated by the weight and machinery size limitations. Thus, the actual operating LP pressure that optimizes the system efficiency will be determined when the compressor size and weight limitations are taken into account.

It is also found that the SEP actuators have to be leveraged to assure that the overall average system pressure is maintained around 7 atm for different loads when air, fuel and steam flows are varied. For example, when the load demand increases, increasing the fuel, air and steam flows without opening the valve of the SEP (i.e. increasing d_o) would result in increased SEP pressure and consequently increased pumping losses.

Finally, at the given inputs the power output is 282 kW. This is calculated based on the FC current demand while the corresponding cell voltage is given by a nominal polarization curve for the specific PEM FC. With that given fuel input, attempting to draw more hydrogen from the SEP by increasing the system pressure will result in decreased overall efficiency and power output.

By repeating the same procedure for different input combinations, one can determine the maximum power output that can be drawn from the system for the entire range of loads up to 500 kW and also determine the optimum mapping of air, fuel, steam and d_o setpoints as functions of the net power. Such mappings can be utilized as a feedforward controller to analyze the open loop performance, as presented in the subsequent section.

5. Open loop system analysis

The main transient performance consideration of the FR–FC system for shipboard application is to assure the safe operation of the system, namely to avoid fuel cell starvation and reactor overheating. In addition, due to the presence of the SEP, it is required to regulate the pressure gradient between the HP and LP sides to prevent excess stress which may lead to membrane rupture.

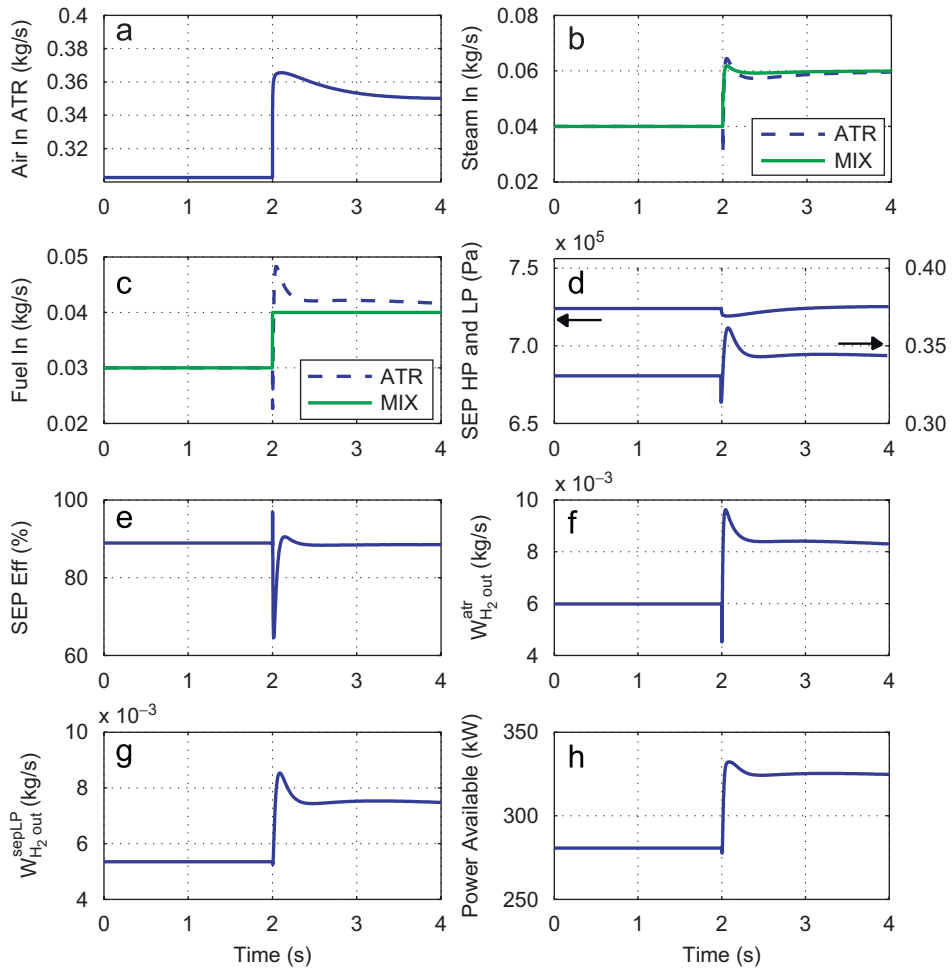

Fig. 6. Open loop response to a 282–320 kW step.

Table 1
Actuator settings for the two steady state power levels illustrated in Fig. 6

Av. power (kW)	Air (kg/s)	Fuel (ks/s)	Steam (ks/s)	d_o (–)
280	0.30	0.03	0.04	0.0030
320	0.35	0.04	0.06	0.0034

In this section the open loop operation of the system is examined during load transitions. Open loop operation is considered when the actuator commands are given via a predetermined feedforward mapping as functions of the net power demand, derived as described in Section 4. Fig. 6 shows the response of different state variables when the net power demand changes from 280 to 320 kW in a step up. The optimal setpoints for the inputs, namely the air, fuel, steam and HP valve of the SEP (d_o), are given in Table 1. Note that when the power demand steps up, all the actuators are stepped up accordingly.

From Fig. 6, it can be seen that even though there is a significant undershoot in the hydrogen production from the ATR (Fig. 6f), no consequential undershoot is observed in the hydrogen going into the FC (Fig. 6g). The ATR hydrogen production undershoot, a similar phenomenon exhibited in the CHP system and examined in [10], can be explained by the λ_{O_2F} and λ_{S_2F} deviations from their desired values during the transient. More elaborate feedback ratio control is required to avoid the ATR H_2 undershoot [10].

The fact that the H_2 production undershoot is mitigated in the system under investigation is a direct result of incorporating the SEP. When a load step is applied to the FC, the hydrogen exiting the LP side is depleted almost instantaneously. This causes an LP pressure drop which immediately increases in SEP efficiency and in turn increases the hydrogen flow through the SEP. Thus, even though the SEP burdens the system with a 7 atm pressure requirement, it benefits the transient performance of the system by acting as a hydrogen buffer.

Similarly, in the case of a step down in the demanded load, as shown in Fig. 7, the overshoot in hydrogen production (Fig. 7f) is not exhibited in the hydrogen flow that is fed to the FC (Fig. 7g) due to the SEP property of filtering out the high-frequency hydrogen flow changes. The undershoot in the hydrogen production (Fig. 7f) though, is due to the discrepancies of the λ_{O_2F} and λ_{S_2F} (mainly due to the undershoot in fuel flow shown in Fig. 7c) and cannot be mitigated by the SEP due to their

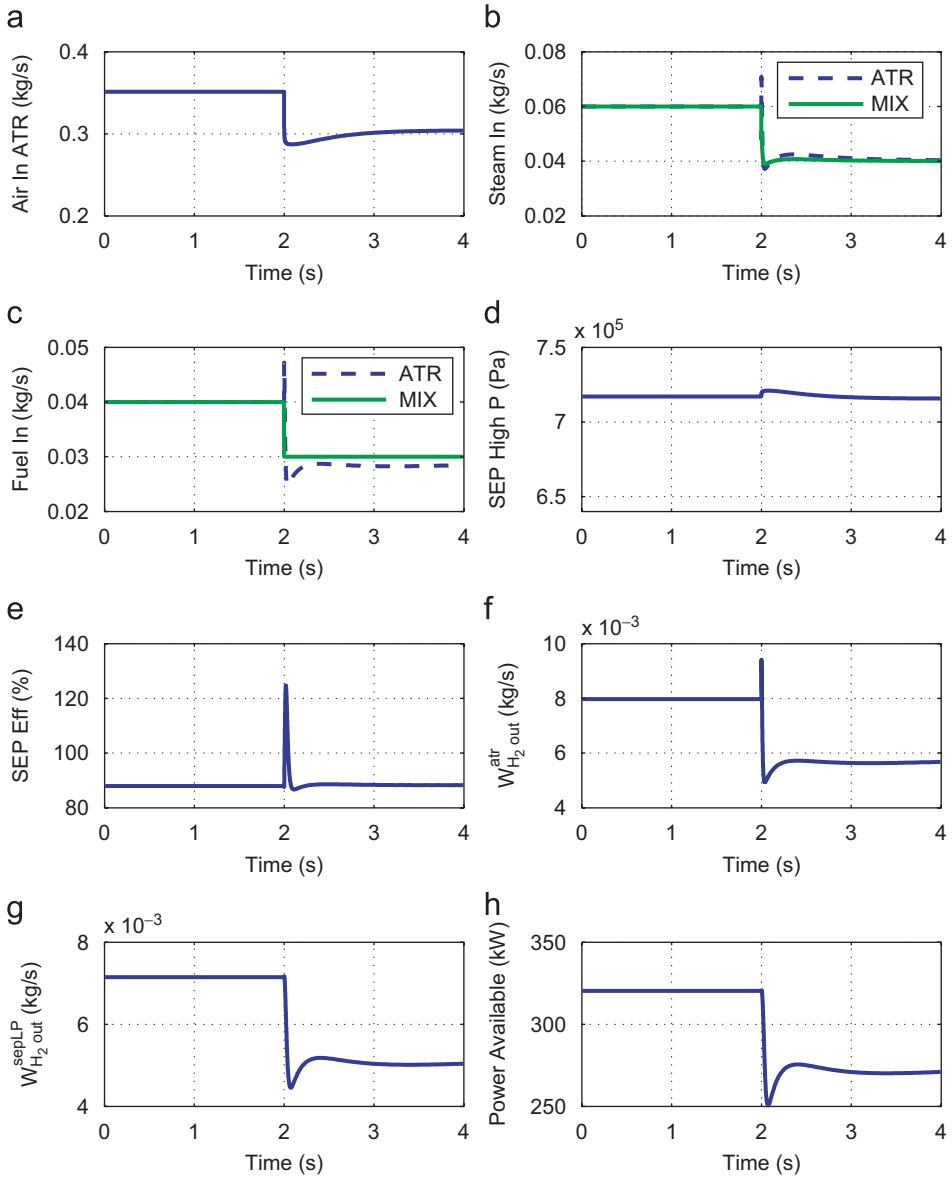

Fig. 7. Open loop response to a 320–282 kW step.

lower frequency and thus propagate to the hydrogen flow that is fed to the FC (Fig. 7g). Eliminating this undershoot would require more sophisticated control of λ_{O_2F} and λ_{S_2F}, which is part of the future work.

Even though the SEP is beneficial to the overall system by acting as a hydrogen buffer, it cannot alleviate ratio discrepancies in the ATR inlet, thus feedback control is required to improve the performance. Furthermore, when uncertainties such as reactor clogging due to aging or fuel composition variability occur, feedback control is essential in maintaining the system's robustness and satisfactory performance [18].

6. Conclusions

In this paper, a dynamic model of an integrated fuel reforming and fuel cell power plant intended for marine applications is presented. The model is based on thermodynamic principles, ideal gas law and energy balance. The chemical products of the ATR are calculated using Gibbs energy minimization. The SEP membrane operation and its effects on overall system performance are analyzed with respect to the LP pressure and the HP outlet valve area. It is shown that a trade off between the SEP efficiency and the overall system efficiency exists and should be considered in the SEP setpoint selection. Furthermore, the open loop response of the system is shown to be satisfactory in terms of the response time and hydrogen production. The fuel starvation problem is mitigated to a large extent during a step up in load, compared to other systems such as the one investigated in [10], thanks to the SEP which introduces a hydrogen storage volume and thus allows smooth supply of hydrogen to the FC. The effects of uncertainties and disturbances on the system performance will be examined

in our future work and the need for feedback control will be assessed.

Acknowledgements

The authors would like to thank S. Miller, J. Heinzel, J. Kuseian, D. Hoffman, E. House, M. Cervi and N. Nelson of NAVSEA Philadelphia and Anna Stefanopoulou from the University of Michigan for their help in developing the model.

References

[1] Chan SH, Wang HM. Thermodynamic and kinetic modelling of an autothermal methanol reformer. J Power Sources 2004;126: 8–15.
[2] Pasel J, Meissner J, Pors Z, Palm C, Cremer P, Peters R, Stolen J. Hydrogen production via autothermal reforming of diesel fuel. Fuel Cells 2004;4(3).
[3] Kamarudin SK, Daud WRW, Som AMd, Mohammad AW, Takriff S, Masdar MS. The conceptual design of a pemfc system via simulation. Chem Eng J 2004;103:99–113.
[4] Hagh BF. Optimization of autothermal reactor for maximum hydrogen production. Int J Hydrogen Energy 2003;28:1369–77.
[5] Ersoz A, Olgun H, Ozdogan S, Gungor C, Akgun F, Týrýs M. Autothermal reforming as a hydrocarbon fuel processing option for pem fuel cell. J Power Sources 2003;118:384–92.
[6] Semelsberger TA, Brown LF, Borup RL, Inbody MA. Equilibrium products from autothermal processes for generating hydrogen-rich fuel-cell feeds. Int J Hydrogen Energy 2004;29:1047–64.
[7] Hoang DL, Chan SH. Modeling of a catalytic autothermal methane reformer for fuel cell applications. Appl Catal A: General 2004;268: 207–16.
[8] Springmann S, Bohnet M, Docter A, Lamm A, Eigenberger G. Cold start simulations of a gasoline based fuel processor for mobile fuel cell applications. J Power Sources 2002;128:13–24.
[9] Pukrushpan JT, Stefanopoulou A, Peng H. Control of fuel cell power systems: principles, modeling, analysis and feedback design. first ed. New York: Springer; 2004.
[10] Tsourapas V, Sun J, Stefanopoulou A. Dynamics, optimization and control of a fuel cell based combined heat power (chp) system for shipboard applications. Am Control Conf 2005.
[11] Sonntag RE, Borgnakke C, Van Wylen GJ. Fundamentals of thermodynamics, sixth ed. New York: Wiley.
[12] http://www.gaseq.co.uk. 2006.
[13] Sonntag RE, Borgnakke C, Van Wylen GJ. Fundamentals of thermodynamics. fifth ed. New York: Wiley; 1998.
[14] Larminie J, Dicks A. Fuel cell systems explained. West Sussex, England: Wiley; 2000.
[15] Martin H. Heat exchangers. Hemisphere Pub. Corp.; 1992.
[16] Communication with P + E Inc. 2005.
[17] Porter KE, Hinchliffe AB, Tighe BJ. Gas separation using membranes—developing a new membrane for the separation of hydrogen and carbon monoxide using the targeting approach. Ind Eng Chem Res 1997;36:830–7.
[18] Tsourapas V, Sun J, Stefanopoulou A. Performance evaluation of a thermally integrated fuel cell system in the presence of uncertainties. ASME Fuel Cell Science, Engineering and Technology, Irvine CA, 2006.